Prediction of localized necking based on crystal plasticity: Comparison of bifurcation and imperfection approaches

Holanyo K. Akpama[1,a], Mohamed Ben Bettaieb[1,2,b] and Farid Abed-Meraim[1,2,c *]

[1]LEM3, UMR CNRS 7239 – Arts et Métiers ParisTech, 4 rue Augustin Fresnel, 57078 Metz Cedex 3, France

[2]DAMAS, Laboratory of Excellence on Design of Alloy Metals for low-mAss Structures, Université de Lorraine, France

[a]holanyo.akpama@ensam.eu, [b]mohamed.benbettaieb@ensam.eu, [c]farid.abed-meraim@ensam.eu

Keywords: Plastic instabilities; Bifurcation theory; Imperfection approach; Crystal plasticity; Self-consistent scale transition; Microstructure–ductility relationships; Forming limit diagrams

Abstract. In the present work, a powerful modeling tool is developed to predict and analyze the onset of strain localization in polycrystalline aggregates. The predictions of localized necking are based on two plastic instability criteria, namely the bifurcation theory and the initial imperfection approach. In this tool, a micromechanical model, based on the self-consistent scale-transition scheme, is used to accurately derive the mechanical behavior of polycrystalline aggregates from that of their microscopic constituents (the single crystals). The mechanical behavior of the single crystals is developed within a large strain rate-independent constitutive framework. This micromechanical constitutive modeling takes into account the essential microstructure-related features that are relevant at the microscale. These microstructural aspects include key physical mechanisms, such as initial and induced crystallographic textures, morphological anisotropy and interactions between the grains and their surrounding medium. The developed tool is used to predict sheet metal formability through the concept of forming limit diagrams (FLDs). The results obtained by the self-consistent averaging scheme, in terms of predicted FLDs, are compared with those given by the more classical full-constraint Taylor model. Moreover, the predictions obtained by the imperfection approach are systematically compared with those given by the bifurcation analysis, and it is demonstrated that the former tend to the latter in the limit of a vanishing size for the initial imperfection.

Introduction

In the field of sheet metal formability, the study and the prediction of plastic strain localization have attracted interest of scientists for a long time. Although a number of valuable contributions have already been published, the modeling and the development of accurate tools for strain localization prediction still remain an active research topic. This research topic has been initiated by the pioneering works of Keeler and Backofen [1] and Goodwin [2], who introduced the concept of forming limit diagram (FLD). The FLD of a sheet metal represents a curve, plotted in the principal strain space, above which localized necking is likely to occur for various strain paths ρ ranging from uniaxial tension ($\rho = -0.5$) to equibiaxial tension ($\rho = 1$). The development of these predictive approaches is based on the coupling between a constitutive framework, to describe the evolution of the variables defining the mechanical state of the studied material, and a localization criterion to predict the onset of localized necking. The first developed predictive models mainly follow a phenomenological description for the mechanical behavior of the studied sheet metals. In this regard, one can quote Hill [3], who used a phenomenological isotropic rigid–plastic model, along with an instability approach nowadays known as Hill's zero-extension criterion, to predict the left-hand side of the FLD. Later, Marciniak and Kuczynski [4] introduced the initial imperfection approach and coupled this localized necking criterion with an isotropic rigid–plastic model in order

to predict the right-hand side of the FLD. Despite their very common use, the phenomenological constitutive models are not able to accurately account for some essential physical aspects of the material behavior, such as initial and induced textures and other microstructure-related parameters (grain morphology, crystallographic structure ...). To overcome these drawbacks, micromechanical modeling can be used instead, for the description of the mechanical behavior of sheet metals. Indeed, the use of advanced and physically-motivated micromechanical models for polycrystalline aggregates allows investigating the impact of microstructures and deformation mechanisms on material ductility, in an attempt of establishing a link between microstructure-related parameters and ductility. This is the approach followed in the present paper to predict ductility limits of polycrystalline aggregates. This prediction is based on the combination of three main components: constitutive modeling at the single crystal scale, a scale-transition scheme to derive the mechanical behavior at the macroscopic level, and a localization criterion to predict the occurrence of localized necking:

- In the current study, a rate-independent approach is adopted to model the mechanical behavior of FCC single crystals. Elasticity is accounted for by using an isotropic linear hypoelastic law, while the plastic flow, which is assumed to be solely due to the shear over the slip systems, is modeled by the Schmid law [5]. An isotropic hardening law is used to express the evolution of the critical shear stresses as a function of the slip rates. This rate-independent formulation is more appropriate when the viscous effects are negligible, which is typically the case in cold forming processes.
- To derive the mechanical behavior of polycrystalline aggregates from the behavior of their microscopic constituents (single crystals), the self-consistent scale-transition scheme is used. This scheme is based on the theoretical developments detailed in Lipinski and Berveiller [6]. Compared to the Taylor model, which is more commonly used in the literature for its simplicity, the use of the self-consistent approach presents several advantageous: the equilibrium condition at the grain level is well respected, and the grain morphology as well as the interactions between the grain and its surrounding medium are accounted for in the modeling.
- Two strain localization criteria are coupled with the self-consistent micromechanical model for the FLD prediction: the imperfection approach, initially developed by Marciniak and Kuczynski [4], and the bifurcation theory, initiated by Rice [7]. Thanks to the Schmid law, which is used to model the plastic flow at the single crystal scale, the application of the bifurcation theory provides realistic levels for the necking strains. This would not be the case if the mechanical behavior was taken rate-dependent. The FLDs predicted by the two localization criteria are compared in the present paper. It is especially demonstrated that the results of the initial imperfection analysis tend towards the bifurcation predictions in the limit of a vanishing size for the geometric imperfection.

The remainder of the paper is organized as follows:

- The constitutive equations describing the single crystal behavior will be developed in the second section.

- In the third section, the theoretical framework of the self-consistent approach will be presented.

- The main equations governing the localization criteria will be exposed in the fourth section.

- Several numerical results and comparisons obtained by the application of the developed tool will be presented and discussed in the fifth section.

Modeling of the single crystal behavior

Let us denote by $\mathbf{g}$ the Eulerian velocity gradient applied at the single crystal scale. The local elastic–plastic constitutive law is defined by means of the tangent modulus $\mathbf{l}$ relating the nominal stress rate $\dot{\mathbf{n}}$ to $\mathbf{g}$ as

$$\dot{\mathbf{n}} = \mathbf{l} : \mathbf{g}. \tag{1}$$

The velocity gradient $\mathbf{g}$ is additively split into its symmetric and anti-symmetric parts, denoted by $\mathbf{d}$ and $\mathbf{w}$, respectively. Under small elastic strain assumption, the strain rate tensor $\mathbf{d}$ and the spin tensor $\mathbf{w}$ are additionally split into their elastic and plastic parts

$$\mathbf{g} = \mathbf{d} + \mathbf{w} \quad ; \quad \mathbf{d} = \mathbf{d}^{e} + \mathbf{d}^{p} \quad ; \quad \mathbf{w} = \mathbf{w}^{e} + \mathbf{w}^{p}. \tag{2}$$

In the present model, the slip on crystallographic planes is considered to be the only source of plastic flow. This constitutive assumption can be expressed as follows:

$$\mathbf{d}^{p} = \sum_{\beta=1}^{N_s} \dot{\gamma}^{\beta} \, \mathrm{sgn}(\tau^{\beta}) \, \mathbf{R}^{\beta} \quad ; \quad \mathbf{w}^{p} = \sum_{\beta=1}^{N_s} \dot{\gamma}^{\beta} \, \mathrm{sgn}(\tau^{\beta}) \, \mathbf{S}^{\beta}, \tag{3}$$

where:

- $\dot{\gamma}^{\beta}$ is the absolute value of the slip rate on the slip system β.
- N_s is the total number of slip systems (equal to 12 for FCC single crystals).
- $\mathbf{R}^{\beta}$ (resp. $\mathbf{S}^{\beta}$) is the symmetric part (resp. anti-symmetric part) of the Schmid orientation tensor.
- τ^{β} is the resolved shear stress for slip system β.

In order to satisfy the objectivity principle, the lattice co-rotational rate $\boldsymbol{\sigma}^{\nabla}$ of the Cauchy stress tensor $\boldsymbol{\sigma}$ is related to the elastic strain rate $\mathbf{d}^{e}$ by the following hypoelastic law:

$$\boldsymbol{\sigma}^{\nabla} = \dot{\boldsymbol{\sigma}} - \mathbf{w}^{e}.\boldsymbol{\sigma} + \boldsymbol{\sigma}.\mathbf{w}^{e} = \mathbf{C}^{e} : \mathbf{d}^{e}. \tag{4}$$

where $\mathbf{C}^{e}$ is the fourth-order elasticity tensor. Elasticity is assumed to be isotropic and is defined by the Young modulus E and the Poisson ratio ν.

The rotation $\mathbf{r}$ of the single crystal lattice frame is defined by the following evolution law:

$$\dot{\mathbf{r}}.\mathbf{r}^{T} = \mathbf{w}^{e}. \tag{5}$$

We introduce the resolved shear stress τ^{β}, which is defined as the projection of the Cauchy stress tensor $\boldsymbol{\sigma}$ on the Schmid orientation tensor

$$\forall \beta = 1, ..., N_s : \quad \tau^{\beta} = \mathbf{R}^{\beta} : \boldsymbol{\sigma}. \tag{6}$$

By using Eqs. 4 and 5, the resolved shear stress rate $\dot{\tau}^{\beta}$ is obtained after some straightforward calculations

$$\forall \beta = 1, ..., N_s : \quad \dot{\tau}^{\beta} = \mathbf{R}^{\beta} : \boldsymbol{\sigma}^{\nabla}. \tag{7}$$

Combining Eqs. 7, 4, and 3, $\dot{\tau}^{\beta}$ can be expressed as

$$\forall \beta = 1, ..., N_s : \quad \dot{\tau}^{\beta} = \mathbf{R}^{\beta} : \mathbf{C}^{e} : \mathbf{d} - \sum_{\alpha=1}^{N_s} \mathrm{sgn}(\tau^{\alpha}) \, \dot{\gamma}^{\alpha} \, \mathbf{R}^{\beta} : \mathbf{C}^{e} : \mathbf{R}^{\alpha}. \tag{8}$$

As mentioned before, the plastic flow at the single crystal scale is governed by the Schmid law [5]. This law states that slip may occur on a given slip system β only if the absolute value of its resolved shear stress τ^{β} reaches a critical value τ_{c}^{β}

$$\forall \beta = 1,...,N_s : \quad \begin{cases} |\tau^\beta| < \tau_c^\beta \Rightarrow \dot{\gamma}^\beta = 0 \\ |\tau^\beta| = \tau_c^\beta \Rightarrow \dot{\gamma}^\beta \geq 0. \end{cases} \tag{9}$$

The initial critical shear stress is assumed to be the same for the different slip systems and it is taken equal to τ_0. The evolution of the critical shear stress τ_c^β is given by the following isotropic hardening law:

$$\forall \beta = 1,...,N_s : \quad \dot{\tau}_c^\beta = h \sum_{\alpha=1}^{N_s} \dot{\gamma}^\alpha \quad ; \quad h = h_0 \left(1 + \frac{h_0 \, \Gamma}{\tau_0 \, n} \right)^{n-1} \quad ; \quad \Gamma = \sum_{\alpha=1}^{N_s} \gamma^\alpha , \tag{10}$$

where h_0 is the initial hardening rate and n is the power-law hardening exponent.

For the different slip systems belonging to the yet-unknown set of active slip systems $\mathcal{A}$, the consistency condition, based on the Schmid law, can be expressed as

$$\forall \beta \in \mathcal{A} : \quad \dot{\chi}^\beta = \dot{\tau}^\beta \, \mathrm{sgn}(\tau^\beta) - \dot{\tau}_c^\beta = 0 \quad , \quad \dot{\gamma}^\beta > 0 . \tag{11}$$

The expression of the slip rates $\dot{\gamma}^\beta$ for the active slip systems can be easily obtained by combining Eqs. 8, 10, and 11

$$\forall \beta \in \mathcal{A} : \quad \dot{\gamma}^\beta = \sum_{\alpha \in \mathcal{A}} M^{\beta\alpha} \mathrm{sgn}(\tau^\alpha) \, \mathbf{R}^\alpha : \mathbf{C}^e : \mathbf{d} = \mathbf{y}^\beta : \mathbf{d} , \tag{12}$$

where $\mathbf{M}$ is the inverse of matrix $\mathbf{P}$ defined by the following index form:

$$\forall \alpha, \beta \in \mathcal{A} : \quad P^{\alpha\beta} = \left(h + \mathrm{sgn}(\tau^\alpha) \, \mathrm{sgn}(\tau^\beta) \, \mathbf{R}^\alpha : \mathbf{C}^e : \mathbf{R}^\beta \right) . \tag{13}$$

Combining the previous equations, the following expression for the microscopic tangent modulus $\mathbf{l}$ can be obtained:

$$\mathbf{l} = \mathbf{C}^e + \boldsymbol{\sigma} \otimes \mathbf{1} - {}^1_{\boldsymbol{\sigma}}\boldsymbol{\Lambda} - {}^2_{\boldsymbol{\sigma}}\boldsymbol{\Lambda} - \sum_{\alpha \in \mathcal{A}} \mathrm{sgn}(\tau^\alpha) \left(\mathbf{C}^e : \mathbf{R}^\alpha + \mathbf{S}^\alpha . \boldsymbol{\sigma} - \boldsymbol{\sigma} . \mathbf{S}^\alpha \right) \otimes \mathbf{y}^\alpha , \tag{14}$$

where $\mathbf{1}$ is the second-order identity tensor, while ${}^1_{\boldsymbol{\sigma}}\boldsymbol{\Lambda}$ and ${}^2_{\boldsymbol{\sigma}}\boldsymbol{\Lambda}$ are fourth-order tensors that contain convective terms of Cauchy stress components

$${}^1_{\boldsymbol{\sigma}}\Lambda_{ijkl} = \frac{1}{2} (\delta_{lj}\sigma_{ik} - \delta_{kj}\sigma_{il}) \quad ; \quad {}^2_{\boldsymbol{\sigma}}\Lambda_{ijkl} = \frac{1}{2} (\delta_{ik}\sigma_{lj} + \delta_{il}\sigma_{kj}) . \tag{15}$$

The constitutive equations at the single crystal scale can be viewed as a strongly non-linear problem, where the main unknowns are the set of active slip systems and the corresponding slip rates. An implicit integration algorithm is developed and used to integrate these constitutive equations. The full details on this integration algorithm are given in [8].

Modeling of the polycrystal behavior

To derive the overall polycrystalline behavior from knowledge of the behavior of individual grains, an incremental version of the self-consistent micromechanical approach is used. Only the main equations of this scale-transition scheme are presented here. Further details on this averaging scheme are given in [6]. The macroscopic behavior law has the same rate form as that of the single crystal (Eq. 1). It allows linking the macroscopic nominal stress rate $\dot{\mathbf{N}}$ to the macroscopic velocity gradient $\mathbf{G}$ by means of the yet-unknown macroscopic tangent modulus $\mathbf{L}$

$$\dot{\mathbf{N}} = \mathbf{L} : \mathbf{G} . \tag{16}$$

The macroscopic velocity gradient and nominal stress rate are defined as the volume averages of their microscopic counterparts

$$\mathbf{G} = \frac{1}{V}\int_V \mathbf{g}\,dV \quad ; \quad \dot{\mathbf{N}} = \frac{1}{V}\int_V \dot{\mathbf{n}}\,dV . \tag{17}$$

To solve the averaging problem, fourth-order concentration tensors, linking macroscopic tensor fields to their microscopic counterparts, are commonly introduced

$$\mathbf{g}(\mathbf{x}) = \mathbf{A}(\mathbf{x}) : \mathbf{G} \quad ; \quad \dot{\mathbf{n}}(\mathbf{x}) = \mathbf{B}(\mathbf{x}) : \dot{\mathbf{N}} . \tag{18}$$

By combining Eq. 1 with Eqs. 16–18, the macroscopic tangent modulus $\mathbf{L}$ can be expressed in the following form:

$$\mathbf{L} = \overline{\mathbf{l}(\mathbf{x}) : \mathbf{A}(\mathbf{x})} , \tag{19}$$

where $\bar{\mathbf{a}}$ is the average of the tensor field $\mathbf{a}$ over the volume of the polycrystal.

The different microscopic mechanical fields are assumed to be homogeneous over each grain. To go further with the derivations, an indicator function θ^I, for each grain I of volume V^I, is defined as

$$\theta^I(\mathbf{x}) = 1 \text{ if } \mathbf{x} \in V^I \quad ; \quad \theta^I(\mathbf{x}) = 0 \text{ if } \mathbf{x} \notin V^I . \tag{20}$$

The local fields can then be expressed in the form

$$\mathbf{g}(\mathbf{x}) = \sum_{I=1}^{N_g} \mathbf{g}^I \theta^I(\mathbf{x}) \quad ; \quad \mathbf{l}(\mathbf{x}) = \sum_{I=1}^{N_g} \mathbf{l}^I \theta^I(\mathbf{x}) , \tag{21}$$

where $\mathbf{g}^I$ (respectively $\mathbf{l}^I$) is the volume average of the velocity gradient (respectively tangent modulus) for grain I, while N_g is the number of grains that make up the studied polycrystalline aggregate. By using Green's tensor, it can be demonstrated, after some elaborate derivations, that the concentration tensor $\mathbf{A}^I$ related to grain I is given by

$$\mathbf{A}^I = (\mathbf{I} - \mathbf{T}^{II} : (\mathbf{l}^I - \mathbf{L}))^{-1} : \overline{(\mathbf{I} - \mathbf{T}^{II} : (\mathbf{l}^I - \mathbf{L}))^{-1}}^{-1} , \tag{22}$$

where $\mathbf{I}$ is the fourth-order identity tensor, and $\mathbf{T}^{II}$ is the interaction tensor for grain I, related to Eshelby's tensor for an ellipsoidal inhomogeneity. In the case of a polycrystalline aggregate comprising N_g grains, with their respective volume fraction f^I, the 1-site self-consistent expression corresponding to the self-consistent scheme in the sense of Hill [9] can be finally obtained as follows:

$$\mathbf{L} = \sum_{I=1}^{N_g} f^I \mathbf{l}^I : \mathbf{A}^I . \tag{23}$$

The set of constitutive equations (16)–(23) represents a non-linear problem, which is solved by using the iterative fixed point method. Note that the full-constraint Taylor model can be easily obtained from the self-consistent constitutive equations, by considering that the concentration tensor $\mathbf{A}^I$ is equal to the fourth-order identity tensor for all grains.

Strain localization criteria

The two localization criteria considered in this study are formulated under the plane-stress conditions, which is justified by the fact that the studied sheet metals are sufficiently thin.

Bifurcation theory. In the current work, the three-dimensional formulation of the bifurcation approach implemented in [10] is adapted to the plane-stress framework. With the plane-stress condition, the macroscopic velocity gradient and nominal stress rate tensor are defined by the following generic forms:

$$\mathbf{G} = \begin{pmatrix} 1 & 0 & 0 \\ 0 & \rho & 0 \\ 0 & 0 & ? \end{pmatrix} \quad ; \quad \dot{\mathbf{N}} = \begin{pmatrix} ? & ? & 0 \\ ? & ? & 0 \\ 0 & 0 & 0 \end{pmatrix}, \tag{24}$$

where ρ is the strain-path ratio, and symbol $?$ designates the unknown components in both tensors. The bifurcation criterion is defined by the singularity of the acoustic tensor, expressed in the following form:

$$\det\left(\vec{\mathcal{N}}^{PS} \,.\mathbf{L}^{PS}.\vec{\mathcal{N}}^{PS}\right) = 0, \tag{25}$$

where:

- $\vec{\mathcal{N}}^{PS}$ is the unit vector normal to the localization band.
- $\mathbf{L}^{PS}$ is the plane-stress tangent modulus, which relates the in-plane components of the nominal stress rate tensor to the in-plane components of the velocity gradient.

The 2D expression $\mathbf{L}^{PS}$ of the tangent modulus is derived from the 3D expression $\mathbf{L}$ by the following condensation relation:

$$\forall \alpha,\beta,\gamma,\delta = 1,2: \quad L^{PS}_{\alpha\beta\gamma\delta} = L_{\alpha\beta\gamma\delta} - \frac{L_{\alpha\beta 33}\, L_{33\gamma\delta}}{L_{3333}}. \tag{26}$$

Initial imperfection approach. The initial imperfection approach (referred to in what follows as the M–K approach) is based on the assumption of the preexistence of an initial geometric imperfection in the form of a narrow band across the thickness of the sheet metal, as illustrated in Fig. 1. Quantities inside (resp. outside) the band are designated by superscript B (resp. H).

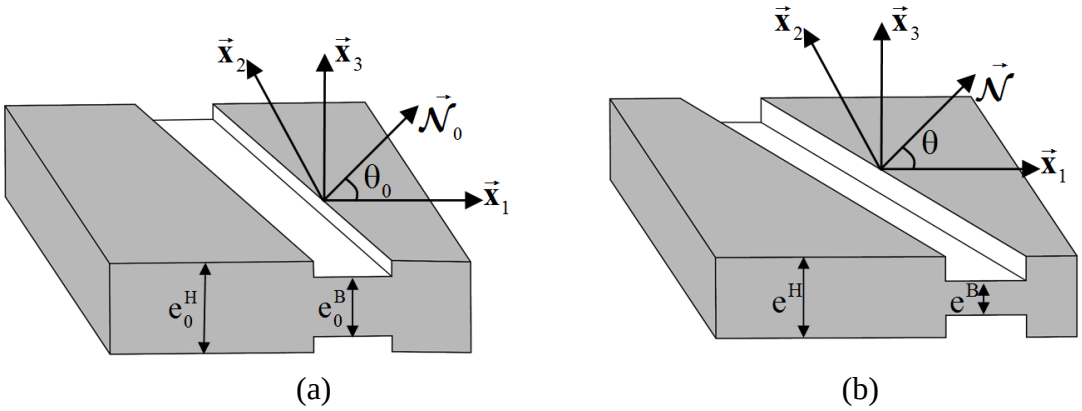

(a) (b)

Fig. 1. M–K analysis for a sheet metal: (a) Initial configuration of the sheet; (b) Current configuration of the sheet.

Both inside and outside the band, the strain and stress fields are assumed to be uniform. The current thickness e^B (resp. e^H) is related to the initial thickness e_0^B (resp. e_0^H) by

$$e^{H} = e_0^{H} \exp(E_{33}^{H}) \quad ; \quad e^{B} = e_0^{B} \exp(E_{33}^{B}), \tag{27}$$

where E_{33}^{B} and E_{33}^{H} are, respectively, the logarithmic strains inside and outside the band in the direction normal to the sheet.

The initial (resp. current) geometric imperfection is measured by the ratio ξ_0 (resp. ξ) defined as

$$\xi_0 = 1 - \frac{e_0^{B}}{e_0^{H}} \quad ; \quad \xi = 1 - \frac{e^{B}}{e^{H}}. \tag{28}$$

This initial (resp. current) imperfection is also characterized by the orientation θ_0 (resp. θ) of the normal vector $\vec{\mathcal{N}}_0^{PS}$ (resp. $\vec{\mathcal{N}}^{PS}$) with respect to the rolling direction of the sheet metal. The evolution law for the localization band orientation θ depends on three quantities: the initial band orientation θ_0, the logarithmic strain outside the band along the rolling direction E_{11}^{H}, and the strain-path ratio ρ

$$\theta = \arctan\left[\tan\theta_0 \exp(1-\rho)\, E_{11}^{H}\right]. \tag{29}$$

In addition to Eqs. 27–29, the M–K analysis is based on three other main equations:

- The kinematic compatibility condition at the interface between the band and the homogeneous zone (i.e., outside the band):

$$\mathbf{G}^{PS\,B} = \mathbf{G}^{PS\,H} + \dot{\vec{\mathbf{C}}}^{PS} \otimes \vec{\mathcal{N}}^{PS}. \tag{30}$$

- The equilibrium equation across the interface between the band and the homogenous zone (expressed in terms of the macroscopic nominal stress rate):

$$e^{B}\, \vec{\mathcal{N}}^{PS}.\dot{\mathbf{N}}^{PS\,B} = e^{H}\, \vec{\mathcal{N}}^{PS}.\dot{\mathbf{N}}^{PS\,H}. \tag{31}$$

- The plane-stress constitutive relations developed in the previous section, expressed inside and outside the band, respectively:

$$\dot{\mathbf{N}}^{PS\,B} = \mathbf{L}^{PS\,B} : \mathbf{G}^{PS\,B} \quad ; \quad \dot{\mathbf{N}}^{PS\,H} = \mathbf{L}^{PS\,H} : \mathbf{G}^{PS\,H}. \tag{32}$$

Using Eq. 32, the equilibrium condition 31 can be expressed in terms of the velocity gradients $\mathbf{G}^{PS\,B}$ and $\mathbf{G}^{PS\,H}$. Then, the compatibility condition 30 can be used to compute the jump vector $\dot{\vec{\mathbf{C}}}^{PS}$

$$\dot{\vec{\mathbf{C}}}^{PS} = \left(\vec{\mathcal{N}}^{PS}.\mathbf{L}^{PS\,B}.\vec{\mathcal{N}}^{PS}\right)^{-1}.\vec{\mathcal{N}}^{PS}.\left[\left(\frac{e^{H}}{e^{B}}\mathbf{L}^{PS\,H} - \mathbf{L}^{PS\,B}\right) : \mathbf{G}^{PS\,H}\right]. \tag{33}$$

Further details on the algorithmic aspects and on the numerical implementation of both localization criteria can be found in [11].

Numerical predictions

Material data. The material parameters corresponding to the modeling at the single crystal scale are given in Table 1 below.

Table 1. Material parameters

Elasticity parameters		Hardening parameters		
E [GPa]	ν	τ_0 [MPa]	h_0 [MPa]	n
210	0.3	40	390	0.2

The studied polycrystalline aggregate is composed of 2000 grains. The initial crystallographic texture is generated randomly and is assumed to be orthotropic (see Fig. 2). All of the grains are assumed to be initially spherical with identical volume fraction.

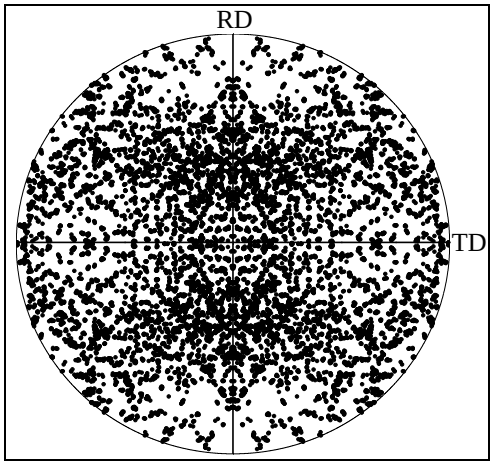

Fig. 2. Initial texture of the studied polycrystalline aggregate: {111} pole figure.

Bifurcation theory results. The evolution of the minimum of the determinant of the acoustic tensor $\vec{\mathcal{N}}^{PS}.\mathbf{L}^{PS}.\vec{\mathcal{N}}^{PS}$, over all possible band orientations θ, as a function of the major strain E_{11} is shown in Fig. 3. In this figure, four representative strain paths are considered ($\rho=-0.5$, $\rho=0$, $\rho=0.5$, and $\rho=1$), and both the self-consistent (SC) approach and the full-constraint (FC) Taylor model are employed to derive the mechanical behavior of the polycrystalline aggregate. It is clear from this figure that the minimum of the determinant of the acoustic tensor abruptly decreases during the transition between the elastic and plastic regimes, which occurs at small strains. By contrast, in the plastic regime, the decrease is much slower. The onset of localized necking is predicted at large plastic strain, when the determinant of the acoustic tensor becomes equal to zero.

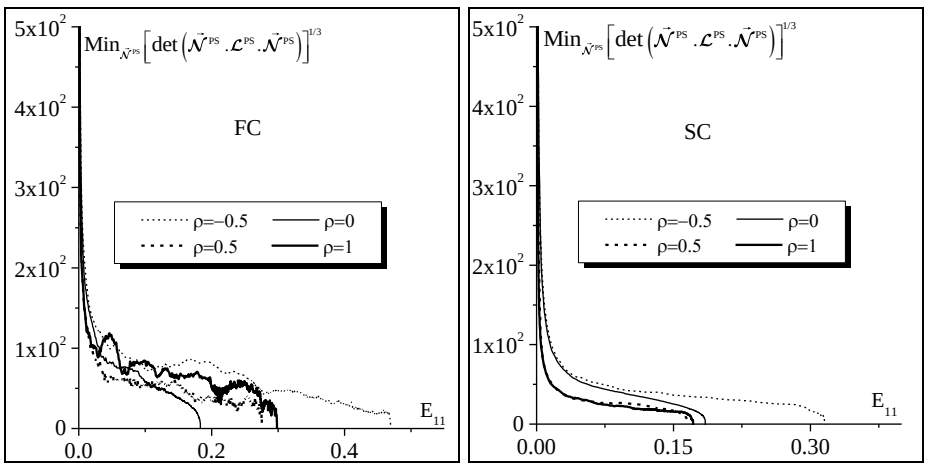

(a) (b)

Fig. 3. Evolution of the minimum of the determinant of the acoustic tensor as a function of E_{11} for four different strain paths ($\rho=-0.5$, $\rho=0$, $\rho=0.5$, and $\rho=1$): (a) FC model; (b) SC model.

The FLDs predicted by the bifurcation criterion, using both the FC and SC models, are shown in Fig. 4a. This figure clearly emphasizes large differences between the FLDs predicted by the two homogenization schemes. Indeed, the limit strains predicted by the FC model are found to be generally much larger than their counterparts predicted by the SC scheme. Fig. 4b shows the necking band orientations θ, as predicted by the two homogenization models, for the different strain paths ρ that span an entire FLD. Although, on the whole, the curves describing the localization band orientation follow an evolution that seems to be qualitatively comparable, there are in fact some significant quantitative differences for the necking band orientations predicted by the two averaging schemes. An important observation is that, unlike the vast majority of FLD approaches based on phenomenological constitutive models, the localization band predicted by using crystal plasticity modeling is not necessarily normal to the direction of major strain for all positive strain paths.

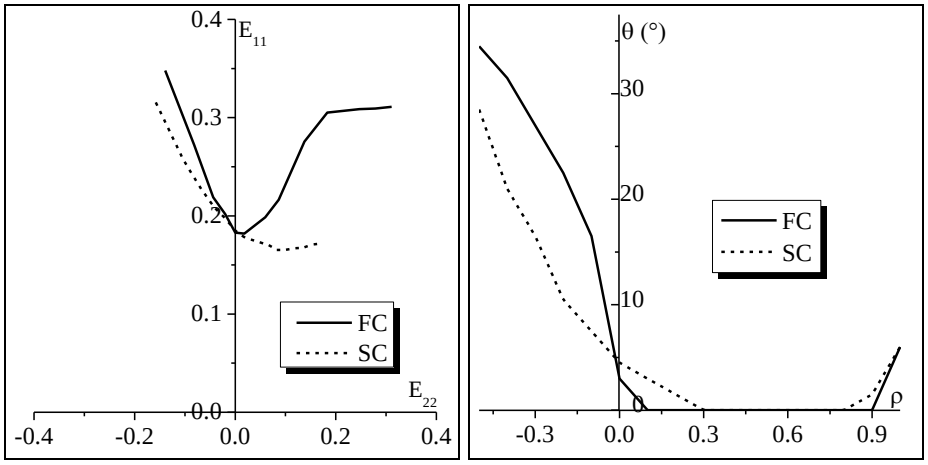

(a) (b)

Fig. 4. FLDs and necking band orientations, as predicted by the FC and SC models coupled with bifurcation theory: (a) FLDs; (b) Necking band orientation for the different strain paths.

Initial imperfection results. The numerical results obtained by the application of the M–K approach are presented in this section. The evolution of the limit strain E_{11} as a function of the initial imperfection size ξ_0 is plotted in Fig. 5 for different strain paths ($\rho = -0.5$, $\rho = 0$, $\rho = 0.5$, and $\rho = 1$). It can be clearly seen that this limit strain E_{11} decreases when the initial imperfection increases.

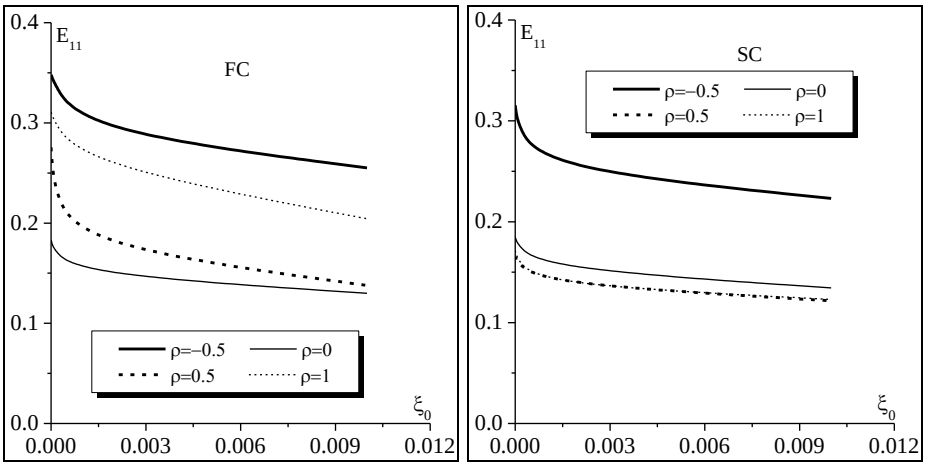

(a) (b)

Fig. 5. Evolution of the limit strain E_{11} as a function of the initial imperfection size ξ_0, for different strain paths ρ: (a) FC model; (b) SC model.

The comparison between the FLDs predicted by bifurcation theory and those determined by M–K analysis is shown in Fig. 6. Three different initial imperfection ratios are considered: $\xi_0 = 10^{-4}$, $\xi_0 = 10^{-3}$, and $\xi_0 = 10^{-2}$. It is found that for all strain paths, the limit strains predicted by bifurcation theory set an upper bound to those yielded by the M–K approach. Moreover, this result is valid for both scale-transition schemes, namely the FC and SC models. Indeed, Fig. 6 demonstrates that the FLDs predicted by the M–K analysis tend towards those determined by bifurcation theory when the size of initial imperfection ξ_0 tends towards zero. In other words, the effect of the initial imperfection is essentially to shift the FLD downwards.

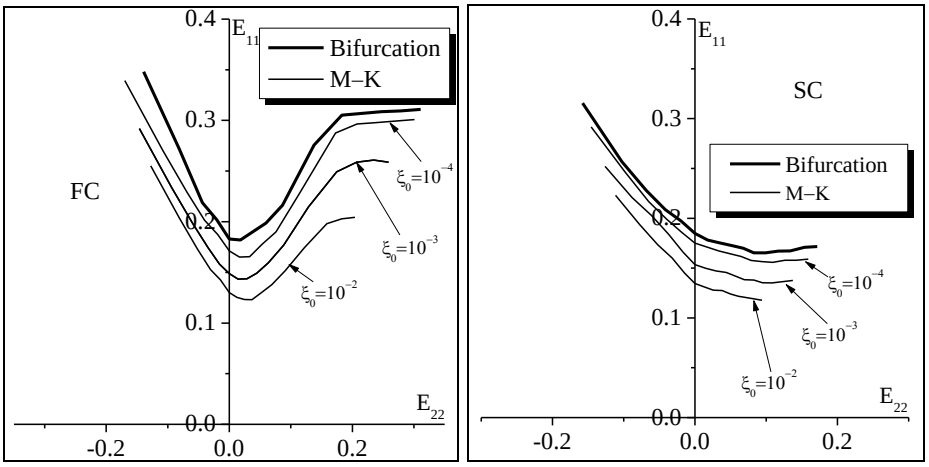

(a) (b)

Fig. 6. Comparison between the FLDs predicted by M–K analysis ($\xi_0 = 10^{-4}$; $\xi_0 = 10^{-3}$; $\xi_0 = 10^{-2}$) and the FLD predicted by bifurcation theory: (a) FC model; (b) SC model.

Concluding remarks

A modeling tool has been developed in this paper to predict the forming limit diagrams for elasto-plastic sheet metals. This tool is based on coupling an advanced micromechanical model with two localized necking criteria. The self-consistent approach is used to derive the mechanical behavior of the polycrystalline aggregate (which is assumed to be representative of the sheet metal)

from knowledge of the mechanical behavior of the individual single crystals. For predicting the limit strains of the polycrystalline aggregate, both the bifurcation theory and the initial imperfection approach have been used. Various numerical simulations have been carried out in order to predict the limit strains and the associated FLDs for polycrystalline materials. From these predictions, it appears that both the shape and the overall level of the FLDs are greatly influenced by the adopted scale-transition scheme. It is also demonstrated that when the initial imperfection size involved in the M–K analysis tends towards zero, the corresponding FLDs tend towards the bifurcation-based FLD.

References

[1] S.P. Keeler, W.A. Backofen, Plastic instability and fracture in sheets stretched over rigid punches, Trans. ASM 56 (1963) 25-48.

[2] G.M., Goodwin, Application of strain analysis to sheet metal forming problems in press shop, Metallurgica Italiana 60 (1968) 767-744.

[3] R. Hill, On discontinuous plastic states, with special reference to localized necking in thin sheets, J. Mech. Phys. Solids 1 (1952) 19-30.

[4] Z. Marciniak, K. Kuczynski, Limit strains in processes of stretch-forming sheet metal, Int. J. Mech. Sci. 9 (1967) 609-620.

[5] E. Schmid, W. Boas, Plasticity of Crystals, Chapman and Hall, London, 1935.

[6] P. Lipinski, M. Berveiller, E. Reubrez, J. Morreale, Transition theories of elastic-plastic deformation of metallic polycrystals, Arch. Appl. Mech. 65 (1995) 291-311.

[7] J.R. Rice, The localization of plastic deformation, in: 14th International Congress of Theoretical and Applied Mechanics, 1976, pp. 207-220.

[8] H.K. Akpama, M. Ben Bettaieb, F. Abed-Meraim, Numerical integration of rate-independent BCC single crystal plasticity models: comparative study of two classes of numerical algorithms, Int. J. Num. Meth. Eng (2016) doi: 10.1002/nme.5215.

[9] R. Hill, Continuum micro-mechanics of elastoplastic polycrystals, J. Mech. Phys. Solids 13 (1965) 89-101.

[10] G. Franz, F. Abed-Meraim, M. Berveiller, Strain localization analysis for single crystals and polycrystals: Towards microstructure-ductility linkage, Int. J. Plasticity 48 (2013) 1-33.

[11] M. Ben Bettaieb, F. Abed-Meraim, Investigation of localized necking in substrate-supported metal layers: Comparison of bifurcation and imperfection analyses, Int. J. Plast. 65 (2015) 168-190.